Complex dispersion relation of surface acoustic waves at a lossy metasurface

Logan Schwan, Alan Geslain, Vicente Romero-García, and Jean-Philippe Groby

Citation: Appl. Phys. Lett. **110**, 051902 (2017); doi: 10.1063/1.4975120
View online: http://dx.doi.org/10.1063/1.4975120
View Table of Contents: http://aip.scitation.org/toc/apl/110/5
Published by the American Institute of Physics

Complex dispersion relation of surface acoustic waves at a lossy metasurface

Logan Schwan,[1,a)] Alan Geslain,[2] Vicente Romero-García,[1] and Jean-Philippe Groby[1]
[1]*LAUM, Université du Maine, UMR CNRS 6613, Le Mans, France*
[2]*ISAT, DRIVE EA1859, Université Bourgogne Franche Comté, Nevers, France*

(Received 17 November 2016; accepted 17 January 2017; published online 31 January 2017)

The complex dispersion relation of surface acoustic waves (SAWs) at a lossy resonant metasurface is theoretically and experimentally reported. The metasurface consists of the periodic arrangement of borehole resonators in a rigid substrate. The theoretical model relies on a boundary layer approach that provides the effective metasurface admittance governing the complex dispersion relation in the presence of viscous and thermal losses. The model is experimentally validated by measurements in the semi-anechoic chamber. The complex SAW dispersion relation is experimentally retrieved from the analysis of the spatial Laplace transform of the pressure scanned along a line at the metasurface. The geometrical spreading of the energy from the speaker is accounted for, and both the real and imaginary parts of the SAW wavenumber are obtained. The results show that the strong reduction of the SAW group velocity occurs jointly with a drastic attenuation of the wave, leading to the confinement of the field close to the source and preventing the efficient propagation of such slow-sound surface modes. The method opens perspectives to theoretically predict and experimentally characterize both the dispersion and the attenuation of surface waves at structured surfaces. *Published by AIP Publishing.* [http://dx.doi.org/10.1063/1.4975120]

While surface waves propagating at the interfaces between two propagative media or at impedance surfaces have been studied theoretically[1–4] and investigated experimentally,[5] they have also been shown to emerge at the surface of impervious media when structured with resonant grooves[6] or boreholes.[7] The parallel between such surface waves and surface plasmons[7] has paved the way to novel applications in imaging,[8,9] focusing,[10] or lensing,[11] for which the dispersion relation of the surface waves can be tuned by designing the micro-structure properties. However, while the dispersion relation of such "spoof surface plasmon" is usually presented for real wavenumbers[12] without accounting for losses, the surface wavenumber is actually a complex quantity, the imaginary part of which accounts for the attenuation of the waves induced by the losses. These latter are unavoidable in practice and govern the magnitude of resonances that can be responsible for bandgaps. If methods to predict theoretically[6,7] the real part of the surface wavenumber and retrieve it experimentally, e.g., from spatial Fourier transform,[13] are now sufficiently robust, retrieving the imaginary part of it can be challenging,[14] notably because it requires to distinguish the attenuation of the wave induced by the losses from that induced by the geometrical spreading of energy in space.

Here, the propagation of surface acoustic waves (SAWs) at a metasurface is investigated both theoretically and experimentally to predict and retrieve in a systematic method both the real and imaginary parts of the complex SAW wavenumber in the presence of the viscous and thermal losses. The theoretical model is based on a Boundary Layer (BL) approach using plane wave expansion, and its predictions are used to validate the complex dispersion relation retrieved experimentally. The metasurface Γ under study consists of the two-dimensional Σ-periodic repetition of circular borehole resonators with the radius a and the depth h, at the otherwise rigid plane surface (see Fig. 1). The resonators are arranged in a square lattice, with the lattice constant ℓ, and the unit lattice vectors ($\mathbf{e}_1$, $\mathbf{e}_2$). Denoting $\mathbf{e}_3 = \mathbf{e}_1 \times \mathbf{e}_2$ the out-of-plane unit vector directed at air, the position vector reads $\mathbf{x} = \mathbf{x}_\Gamma + x_3\mathbf{e}_3$, where $\mathbf{x}_\Gamma = x_1\mathbf{e}_1 + x_2\mathbf{e}_2$ is the projection of $\mathbf{x}$ on Γ. The SAW propagation at the surface Γ is studied in the linear harmonic regime at the circular frequency ω (time convention $e^{-i\omega t}$), and under the ambient conditions, with the air density ρ_e, the atmospheric pressure P_e, the adiabatic constant γ, the viscosity η, the Prandtl number Pr, the sound speed $c = \sqrt{\gamma P_e/\rho_e}$, and the air wavenumber $k_0 = \omega/c$. The BL analysis is performed for the SAW with the pressure $p = Pe^{i\mathbf{k}\cdot\mathbf{x}_\Gamma - bx_3}$, where P is the complex amplitude, $\mathbf{k} = k\mathbf{e}_\alpha$ is the in-plane wave-vector with the complex wavenumber k and the in-plane unit vector $\mathbf{e}_\alpha$, which makes the angle α counted from $\mathbf{e}_1$, and where $b = \sqrt{k^2 - k_0^2}$ is the complex attenuation parameter in the direction $\mathbf{e}_3$. For actual

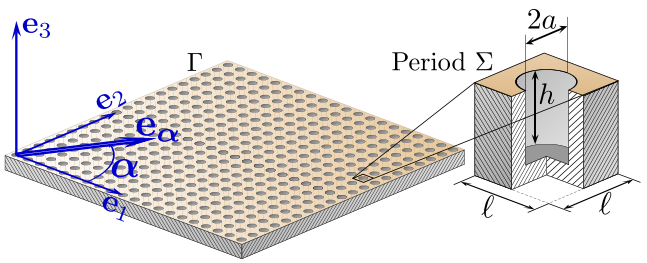

FIG. 1. Schematic of the Σ-periodic metasurface and details of the unit cell (lattice size ℓ) bearing a $2a$-diameter and h-deep borehole resonator. $\mathbf{e}_1$ and $\mathbf{e}_2$ are the unit lattice vectors; $\mathbf{e}_3$ is the normal vector; and $\mathbf{e}_\alpha$ gives the direction of the SAW propagation.

a)Electronic mail: logan.schwan@gmail.com

propagation along $\mathbf{e}_\alpha$ and wave attenuation, the following conditions hold: $\mathrm{Re}\,(k) \geq 0$, $\mathrm{Im}\,(k) \geq 0$ and $\mathrm{Re}\,(b) \geq 0$.

When excited by p, the resonators act as mutually interacting secondary sources that prescribe the distribution of normal velocity $v_\Gamma \mathbf{e}_3$ at the surface Γ. Emitted by the periodic lattice while forced by the SAW, the velocity v_Γ is locally Σ-periodic, while modulated by the factor $e^{\mathrm{i}\mathbf{k}\cdot\mathbf{x}_\Gamma}$. Since the SAW cannot resolve the array periodicity on its own, locally Σ-periodic perturbations localized in the vicinity of Γ are induced, which can be described in the low frequency range (typically $k_0\ell < 2\pi$) by a BL[15,16] with the pressure $p^\star$ in the form

$$p^\star = \sum_{(n,q)\neq(0,0)} P^\star_{nq} e^{\mathrm{i}(\mathbf{k}+\mathbf{G}_{nq})\cdot\mathbf{x}_\Gamma - b^\star_{nq} x_3}, \tag{1}$$

where n and q are integers, $P^\star_{nq}$ are complex scattering coefficients, $\mathbf{G}_{nq} = 2\pi(n\mathbf{e}_1 + q\mathbf{e}_2)/\ell$ are the reciprocal lattice vectors, and $b^\star_{nq} = \sqrt{(\mathbf{k}+\mathbf{G}_{nq})^2 - k_0^2}$ are the complex out-of-plane attenuation parameters with $\mathrm{Re}\,(b^\star_{nq}) \geq 0$. The dispersion relation is found from the following boundary conditions that have to be satisfied by the superposition of the surface wave p and the BL pressure $p^\star$. At the reference cell Σ, the surface is rigid, except for the borehole aperture S at its center, where a uniform particle velocity $v_o\ \mathbf{e}_3$ is assumed in the long-wavelength approximation.[17] The velocity v_o is then related to the mean value $\langle p + p^\star\rangle = |S|^{-1} \int_S (p + p^\star)\,\mathrm{d}S$ of the pressure $p + p^\star$ acting at the aperture S through the frequency-dependent admittance Y of the resonator, that is, $v_o = Y\langle p + p^\star\rangle$. For the quarter-wavelength resonator, the admittance Y takes the form (see supplementary material for details)

$$Y = \mathrm{i}\tan(\omega h/\sqrt{B^*/\rho^*})/\sqrt{\rho^* B^*}, \tag{2}$$

where ρ^* and B^* are the complex effective density and bulk modulus in the resonator. They account for the viscous and thermal losses in the circular borehole and are classically given by[18,19]

$$\rho^* = \frac{\rho_e}{1 - F\left(\sqrt{2\mathrm{i}}\,\frac{a}{\delta_v}\right)}; \quad B^* = \frac{\gamma P_e}{1 + (\gamma-1)F\left(\sqrt{2\mathrm{i}}\,\frac{a}{\delta_t}\right)}, \tag{3}$$

where $\delta_v = \sqrt{\eta/(\rho_e\omega)}$ and $\delta_t = \delta_v/\sqrt{\mathrm{Pr}}$ are viscous and thermal skin-depths, and $F(y) = 2\mathrm{J}_1(y)/[y\mathrm{J}_0(y)]$ is a form function[18,19] with J_n the Bessel function of order n. The admittance Y is thus complex for the lossy resonators. Now, denoting Π_S the gate function equal to 1 over S and 0 elsewhere at Σ, the boundary conditions at the reference cell can be summarized as

$$\frac{\partial(p+p^\star)}{\partial x_3} = \mathrm{i}k_0\rho_e c Y\langle p + p^\star\rangle\Pi_S \quad \text{at} \quad \Sigma. \tag{4}$$

First, the mean pressure over the aperture S reads

$$\langle p + p^\star\rangle = P\mathcal{H}_{00} + \sum_{(n,q)\neq(0,0)} P^\star_{nq}\mathcal{H}_{nq}, \tag{5}$$

where the structure factors $\mathcal{H}_{nq}$ are given by

$$\mathcal{H}_{nq} = \frac{1}{|S|}\int_S e^{\mathrm{i}(\mathbf{k}+\mathbf{G}_{nq})\cdot\mathbf{x}_\Gamma}\,\mathrm{d}S = \frac{\mathrm{J}_1(K_{nq}a)}{K_{nq}a/2}, \tag{6}$$

with $K_{nq} = \sqrt{(\mathbf{k}+\mathbf{G}_{nq})^2}$. Next, multiplying Eq. (4) by $e^{-\mathrm{i}(\mathbf{k}+\mathbf{G}_{ms})\cdot\mathbf{x}_\Gamma}$, where (m, s) are integers, and taking the mean value over the period Σ yield Equations (7a) and (7b) for $(m, s) = (0, 0)$ and $(m, s) \neq (0, 0)$, respectively

$$-bP = \mathrm{i}k_0\frac{\rho_e c Y|S|}{|\Sigma|}\langle p + p^\star\rangle\mathcal{F}_{00}, \tag{7a}$$

$$-b^\star_{ms}P^\star_{ms} = \mathrm{i}k_0\frac{\rho_e c Y|S|}{|\Sigma|}\langle p + p^\star\rangle\mathcal{F}_{ms}, \tag{7b}$$

where the structure factors $\mathcal{F}_{ms}$ read

$$\mathcal{F}_{ms} = \frac{1}{|S|}\int_S e^{-\mathrm{i}(\mathbf{k}+\mathbf{G}_{ms})\cdot\mathbf{x}_\Gamma}\,\mathrm{d}S = \frac{\mathrm{J}_1(K_{ms}a)}{K_{ms}a/2}. \tag{8}$$

Combining Eqs. (5) and (7b) provides the equation satisfied by the BL scattering coefficients. Re-arranging the double-indexation $(n, q) \neq (0, 0)$ into a single indexation, the following vectors are defined, $\{P^\star\} = \mathrm{vect}(P^\star_{nq})$, $\{\mathcal{H}\} = \mathrm{vect}(\mathcal{H}_{nq})$, and $\{\mathcal{F}\} = \mathrm{vect}(\mathcal{F}_{nq})$, and the diagonal matrix $[b^\star] = \mathrm{diag}(b^\star_{nq})$. With those notations, the BL scattering coefficients are given by

$$\{P^\star\} = -\mathrm{i}k_0\frac{\rho_e c Y|S|}{|\Sigma|}\mathcal{H}_{00}P[\mathcal{B}^\star]^{-1}\{\mathcal{F}\}, \tag{9}$$

where the matrix $[\mathcal{B}^\star]$ reads, with $\otimes$ the tensor product

$$[\mathcal{B}^\star] = [b^\star] + \mathrm{i}k_0\frac{\rho_e c Y|S|}{|\Sigma|}\{\mathcal{F}\}\otimes\{\mathcal{H}\}. \tag{10}$$

Combining Eqs. (5), (7a) and (9), the boundary condition for the SAW takes the form $\partial p/\partial x_3 = -\mathrm{i}\omega\rho_e\Upsilon p$ at Γ, where the effective normalized admittance is

$$\rho_e c\Upsilon = -\frac{\rho_e c Y|S|}{|\Sigma|}\left(1 - \mathrm{i}k_0 d^\star\frac{\rho_e c Y S}{|\Sigma|}\right)\mathcal{F}_{00}\mathcal{H}_{00}, \tag{11}$$

with the scalar $d^\star = \{\mathcal{H}\}\cdot\{[\mathcal{B}^\star]^{-1}\{\mathcal{F}\}\}$ having the dimension of a length. More details about the derivation of Eqs. (9)–(11) are provided in the supplementary material. Eq. (11) provides the micro/macro relation between the resonator properties and the effective admittance actually resolved by the SAW. The SAW dispersion relation is found by solving for k in the equation $b = \mathrm{i}k_0\rho_e c\Upsilon$, which shows that b and hence the wavenumber k are complex quantities when the admittance Υ is not purely imaginary, which is the case for lossy resonators.

In the experiments, the resonators consist of circular boreholes with the radius $a = 18 \pm 0.5$ mm and the depth $h = 40.5 \pm 0.5$ mm drilled with the lattice size ℓ in a rigid wooden substrate. Such quarter-wavelength resonator, with the undamped eigenfrequency $\omega_o/(2\pi) = c/(4h) \approx 2117$ Hz, has been characterized in the impedance tube with the square cross-section $\Sigma = 42\,\mathrm{mm} \times 42\,\mathrm{mm}$ that enables to emulate plane wave reflection at normal incidence on

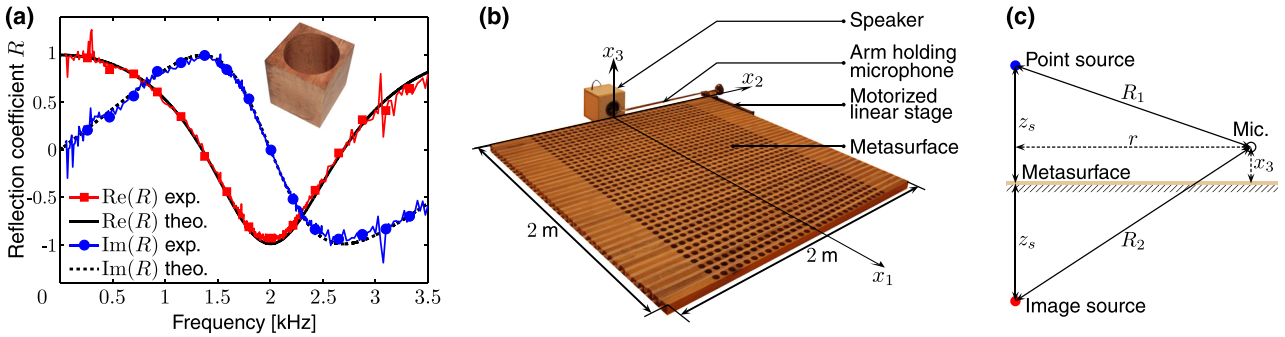

FIG. 2. (a) Comparison of the real and imaginary parts of the reflection coefficient provided by the impedance tube measurements—exp.—on a 42 mm $\times$ 42 mm unit cell (see inset) and those provided by the theoretical effective admittance—theo.—(b) Experimental set-up for characterisation of SAW propagation at the metasurface prototype. (c) Model of the experimental set-up by a point source and a microphone—Mic.—above the metasurface admittance.

the metasurface with an infinite extent. Noting that the effective admittance $\rho_e c \Upsilon$ is also valid for plane wave reflection, the reflection coefficient measured experimentally is compared with the theoretical one $R = [1 - \rho_e c \Upsilon]/[1 + \rho_e c \Upsilon]$ in Fig. 2(a). The results confirm the accuracy of Eqs. (2) and (11) to describe the lossy resonators and the effective metasurface admittance.

To investigate the SAW propagation at the metasurface, semi-anechoic chamber measurements have been performed. The metasurface consists of 1160 resonators (40 along $\mathbf{e}_1 \times 29$ along $\mathbf{e}_2$) drilled periodically with the lattice size $\ell = 50 \pm 1$ mm in a 2 m $\times$ 2 m rigid wooden board (see Fig. 2(b)). The speaker has been positioned at the center of the smaller edge ($x_1 = 0 = x_2$) with the center of its membrane at $z_s \approx 7.5$ cm above the metasurface. The system has been excited with a sine-sweep signal over the frequency range [0.1; 1.6] kHz, in order to focus on the frequency range, wherein the SAW mode theoretically exists according to the BL model (see Fig. 3). The pressure field has been measured with the microphone secured to a motorized linear stage. The experimental spectra have been recorded with the Dynamic Signal Analyzer (Stanford Research Systems type SR785) every 0.5 cm along the line $x_2 = 0$ at the distance $x_1 \in [x_0; L] = [5; 180]$ cm from the speaker and at $x_3 \approx 1$ cm above the surface.

Due to the geometrical spreading of the field from the speaker, the experimental set-up is modelled as a point-source above the metasurface admittance. Hence, the sound field consists of the pressure $p_s(\mathbf{x}) = A_0 \mathcal{G}_0(\mathbf{x}) + A_s \mathcal{G}_s(\mathbf{x})$, where A_0 and A_s are complex amplitudes, $\mathcal{G}_0$ is the Green function for the point source above the rigid surface, and $\mathcal{G}_s$ is the perturbation produced by the metasurface admittance, including the SAW[3]

$$\mathcal{G}_0 = e^{ik_0 R_1}/(4\pi R_1) + e^{ik_0 R_2}/(4\pi R_2), \tag{12a}$$

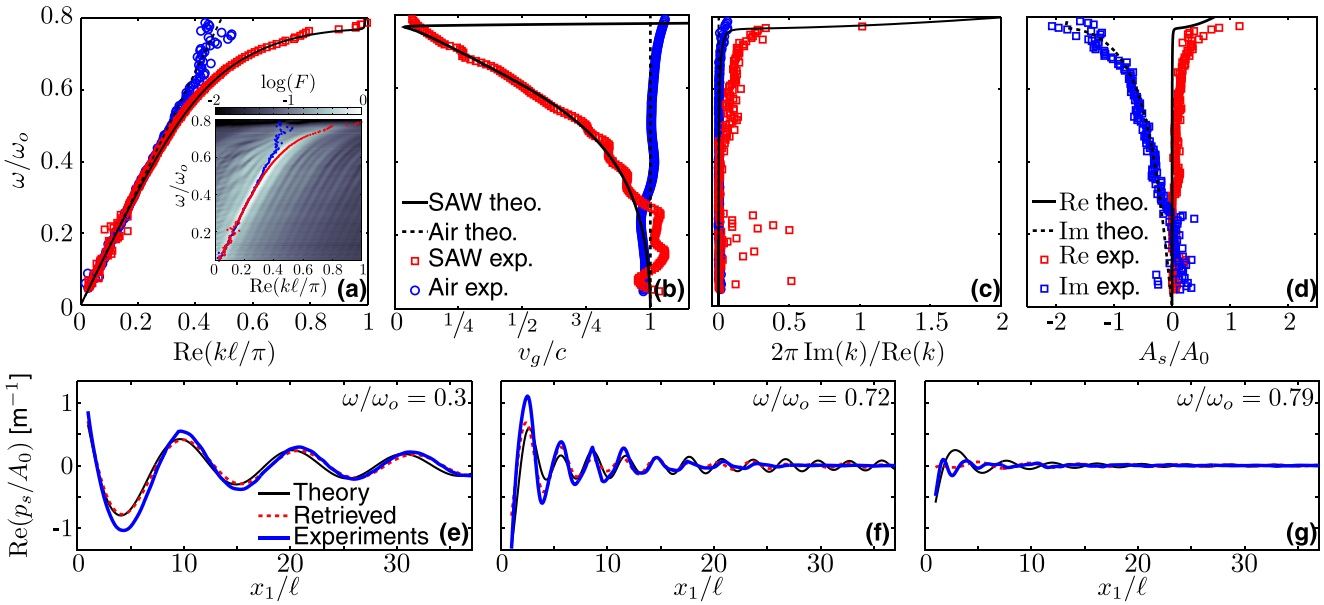

FIG. 3. Comparison between theoretical (theo.) and experimental (exp.) results. Plotted against the normalized frequency ω/ω_o are: (a) the real part and (c) the imaginary part of the air and SAW wavenumbers; (b) the normalized group velocity; (d) the amplitude ratio between the SAW and the air modes. Plotted against the normalized distance x_1/ℓ from the speaker are: (e)–(g) the pressure profile along the scan-line at three frequencies. (a) and (c) have the same legend as (b). (f) and (g) have the same legend as (e). The inset in (a) shows the spatial Fourier transform of the experimental pressure against the frequency and the dispersion relations retrieved from the SLaTCoW method.

$$\mathcal{G}_s = -k_0\,\mathrm{erfc}(-\mathrm{iw})\mathrm{H}_0^{(1)}(kr)e^{-b(x_3+z_s)}/4. \quad (12b)$$

Here, the geometrical parameters R_1, R_2, and r are defined in Fig. 2(c); erfc is the complementary error function; $\mathrm{H}_0^{(1)}$ is the Hankel function of the first kind and order 0; and $\mathrm{w} = \sqrt{\mathrm{i}k_0R_2 - \mathrm{i}kr + b(x_3+z_s)}$ is the numerical distance. Eq. (12) shows that the field $p_s(\mathbf{x})$ vanishes as the distance from the speaker increases: the field $\mathcal{G}_0$ decreases typically as $1/R_1$, while the term $\mathrm{H}_0^{(1)}(kr)e^{-b(x_3+z_s)}$ in the expression of $\mathcal{G}_s$ decreases as $1/\sqrt{r}$. Using the pressure $p_s(\mathbf{x})$ as the ansatz field, and hence accounting for the geometrical spreading from the source, the real and imaginary parts of the wavenumbers k_0 and k, and the complex amplitudes A_0 and A_s are retrieved from the experimental data by means of the *Spatial Laplace Transform for Complex Wavenumbers*—SLaTCoW—method[14] (see supplementary material for more details about the SLaTCoW procedure). The experimental results are compared with those from the BL model in Figs. 3(a)–3(d), where the complex wavenumbers, the group velocity $v_g = \mathrm{d}\omega/\mathrm{dRe}\,(k)$ and the amplitude ratio A_s/A_0 (theoretically equal to[3] $\rho_e c\Upsilon$) have been plotted against the frequency.

While the air line $\mathrm{Re}\,(k_0) = \omega/c$ with the sound speed $c \approx 342$ m/s, and negligible attenuation, $2\pi\mathrm{Im}\,(k_0)/\mathrm{Re}\,(k_0) \sim 5\times10^{-3}$, are recovered, three regimes can be identified in the SAW dispersion relation: at low frequency $\omega \ll \omega_o$, around the resonance $\omega \to \omega_o$ with $\mathrm{Re}\,(k) < \pi/\ell$, and around the Bragg limit $\mathrm{Re}\,(k) \to \pi/\ell$.

In the low-frequency regime, the low admittance contrast $|\rho_e c\Upsilon| \ll 1$ leads the complex SAW dispersion relation $k(\omega)$ to be asymptotic to that of air $k_0(\omega)$. Although it allows an actual propagation of the SAW with negligible attenuation, its contribution in the field remains limited due to its low amplitude $|A_s/A_0| \ll 1$. Besides, this low value of the SAW amplitude makes it difficult to retrieve the mode experimentally, which can explain the scattered experimental data below $\omega/\omega_o = 0.2$. In contrast, around the resonance at $\omega/\omega_o \sim 0.7$, the significant admittance contrast $|\rho_e c\Upsilon| \sim 1$ results in the deviation of the SAW dispersion relation from the air-line. The SAW group velocity decreases down to $v_g/c \sim 1/5$, while the SAW wavelength becomes $\approx 1/8$ of the characteristic attenuation length $1/\mathrm{Im}\,(k)$. That enables the actual propagation of the "slow sound" SAW that could be used for sub-wavelength imaging, for instance. Note that the resonant behavior of the surface microstructures is essential for this phenomenon to occur, since it is responsible for the significant admittance contrast $|\rho_e c\Upsilon| \sim 1$ at the origin of the SAW excitation. However, the capacity to guide waves along the surface with such a "slow sound" is rapidly hindered by the SAW attenuation, as the dispersion curve approaches the Bragg limit $\mathrm{Re}\,(k) \to \pi/\ell$. As the group velocity approaches zero, the SAW attenuation increases drastically with a characteristic attenuation length $1/\mathrm{Im}\,(k)$ of the order of the SAW wavelength, which prevents the effective propagation of the wave at the surface. Note that the interaction of the resonance-induced dispersion relation with the Bragg limit $\mathrm{Re}\,(k) = \pi/\ell$ makes the "bandgap" occur at $\omega/\omega_o \approx 0.8$. Lowering the resonance frequency would certainly make the dispersion relation cross the Bragg limit at the resonance frequency $\omega/\omega_o \approx 1$.

The retrieved dispersion relation is in good agreement with the maxima of the experimental spatial Fourier transform $F(k_r) = \int_{x_0}^{L} p_s/A_0 e^{-\mathrm{i}k_r x_1}\mathrm{d}x_1$ plotted in the inset of Fig. 3(a). This latter also exhibits clearly the regime of highly attenuated waves around $\omega/\omega_o \approx 0.8$, wherein $|F(k_r)| \to 0$. The experimental results are also in well agreement with the theoretical model derived for plane waves. It highlights the accuracy of the effective admittance $\rho_e c\Upsilon$ and underlines that the complex dispersion relation is related more to the metasurface admittance and less to the nature of the excitation.

Finally, Figs. 3(e)–3(g) show the pressure profile $\mathrm{Re}\,(p_s/A_0)$ for frequencies in each SAW propagation regime. It is compared with the profile computed using either the effective admittance $\rho_e c\Upsilon$ or the parameters retrieved from the SLaTCoW method. A good agreement is reached between them. Discrepancies between the theoretical and experimental results in Fig. 3(g) can be due to the conjugate effect of near-fields produced by the speaker in its close-vicinity (where the field is actually confined), and the low level of the signal near the bandgap. Nevertheless, the results show the strong confinement of the field close to the speaker as the frequency increases. That suggests that tracking pulses on distances sufficiently long to perform imaging could be more challenging than in optics.[20]

In conclusion, a boundary layer model that enables to find the effective surface condition satisfied by plane waves at the metasurface has been proposed, which takes full account of multiple interactions, surface periodicity, and viscothermal losses in the resonators. The complex dispersion relation theoretically derived has served to validate that experimentally retrieved using the SLaTCoW method, adapted for point-source excitation. The results have exhibited the mode conversion that occurs between bulk and surface waves in the presence of the metasurface, and they have shown that SAW propagation, while strongly slowed around the resonance, can become drastically attenuated even with weakly damped resonators, hence preventing actual propagation. This underlines the importance of considering the imaginary part of wavenumbers when designing spoof surface plasmon acoustic devices.

See supplementary material for more details about the boundary layer model and the adaptation of the SLaTCoW procedure to the problem of the point source above the metasurface admittance.

The authors are grateful to the French ANR project Metaudible (ANR-13-BS09-0003) and the COST Action DENORMS-CA15125, supported by COST (European Cooperation in Science and Technology).

[1]K. A. Norton, Proc. IRE **24**, 1367 (1936).
[2]A. R. Wenzel, J. Acoust. Soc. Am. **55**, 956 (1974).
[3]C. F. Chien and W. W. Soroka, J. Sound Vib. **43**, 9 (1975).
[4]K. Attenborough, S. I. Hayek, and J. M. Lawther, J. Acoust. Soc. Am. **68**, 1493 (1980).
[5]D. G. Albert, J. Acoust. Soc. Am. **113**, 2495 (2003).
[6]L. Kelders, J. F. Allard, and W. Lauriks, J. Acoust. Soc. Am. **103**, 2730 (1998).
[7]J. B. Pendry, L. Martín-Moreno, and F. J. Garcia-Vidal, Science **305**, 847 (2004).
[8]H. Jia, M. Lu, Q. Wang, M. Bao, and X. Li, Appl. Phys. Lett. **103**, 103505 (2013).
[9]H. Jia, M. Lu, X. Ni, M. Bao, and X. Li, J. Appl. Phys. **116**, 124504 (2014).

[10]Y. Ye, M. Ke, Y. Li, T. Wang, and Z. Liu, J. Appl. Phys. **114**, 154504 (2013).
[11]M. Addouche, M. A. Al-Lethawe, A. Choujaa, and A. Khelif, Appl. Phys. Lett. **105**, 023501 (2014).
[12]D. Torrent and J. Sánchez-Dehesa, Phys. Rev. Lett. **108**, 174301 (2012).
[13]Z. He, H. Jia, C. Qiu, Y. Ye, R. Hao, M. Ke, and Z. Liu, Phys. Rev. B **83**, 132101 (2011).
[14]A. Geslain, S. Raetz, M. Hiraiwa, M. A. Ghanem, S. P. Wallen, A. Khanolkar, N. Boechler, J. Laurent, C. Prada, A. Duclos, P. Leclaire, and J.-P. Groby, J. Appl. Phys. **120**, 135107 (2016).
[15]C. Boutin and P. Roussillon, Int. J. Eng. Sci. **44**, 180 (2006).
[16]C. L. Holloway and E. F. Kuester, Radio Sci. **35**, 661, doi:10.1029/1999RS002162 (2000).
[17]C. Lagarrigue, J.-P. Groby, V. Tournat, O. Dazel, and O. Umnova, J. Acoust. Soc. Am. **134**, 4670 (2013).
[18]C. Zwikker and C. W. Kosten, *Sound Absorbing Materials* (Elsevier Publishing Company, Inc., 1949).
[19]M. R. Stinson, J. Acoust. Soc. Am. **89**, 550 (1991).
[20]H. Gersen, T. J. Karle, R. J. P. Engelen, W. Bogaerts, J. P. Korterik, N. F. van Hulst, T. F. Krauss, and L. Kuipers, Phys. Rev. Lett. **94**, 073903 (2005).